Gas- and plasma-driven hydrogen permeation behavior of stagnant eutectic-solid GaInSn/Fe double-layer structure

Wen-Na Jing(荆文娜)[1], Jian-Xing Liu(刘建星)[1], Heng-Xin Guo(郭恒鑫)[1], Si-Shu Wang(王思蜀)[2], Hai-Lin Bi(毕海林)[3], Bo Chen(陈波)[1], Jian-Jun Chen(陈建军)[1], Hong-Bin Wang(王宏彬)[1], Jian-Jun Wei(韦建军)[2], Zong-Biao Ye(叶宗标)[1,†], and Fu-Jun Gou(芶富均)[1,‡]

[1] *Key Laboratory of Radiation Physics and Technology of the Ministry of Education, Institute of Nuclear Science and Technology, Sichuan University, Chengdu* 610064, *China*
[2] *Institute of Atomic and Molecular Physics, Sichuan University, Chengdu* 610064, *China*
[3] *Hefei University of Technology, Hefei* 230009, *China*

(Received 21 June 2022; revised manuscript received 23 August 2022; accepted manuscript online 21 September 2022)

Gas-driven permeation (GDP) and plasma-driven permeation (PDP) of hydrogen gas through GaInSn/Fe are systematically investigated in this work. The permeation parameters of hydrogen through GaInSn/Fe, including diffusivity, Sieverts' constant, permeability, and surface recombination coefficient are obtained. The permeation flux of hydrogen through GaInSn/Fe shows great dependence on external conditions such as temperature, hydrogen pressure, and thickness of liquid GaInSn. Furthermore, the hydrogen permeation behavior through GaInSn/Fe is well consistent with the multi-layer permeation theory. In PDP and GDP experiments, hydrogen through GaInSn/Fe satisfies the diffusion-limited regime. In addition, the permeation flux of PDP is greater than that of GDP. The increase of hydrogen plasma density hardly causes the hydrogen PDP flux to change within the test scope of this work, which is due to the dissolution saturation. These findings provide guidance for a comprehensive and systematic understanding of hydrogen isotope recycling, permeation, and retention in plasma-facing components under actual conditions.

Keywords: liquid metals, double-layer, gas-driven permeation, plasma-driven permeation

PACS: 52.40.Hf, 67.63.–r, 68.03.–g **DOI:** 10.1088/1674-1056/ac9365

1. Introduction

In fusion devices, the heat load and particle handling of plasma-facing materials (PFMs) are two of the significant engineering application problems. Liquid metals are outstanding in high thermal conductivity, low operating pressure, simple cycle extraction of tritium, and self-healing property.[1] These properties of liquid metals can effectively mitigate the effects of the heat load and particles. As for the feasibility, liquid metals have been testified in nuclear fusion devices including NSTX,[2] EAST,[3] and FTU.[4] The heat load limit of liquid metal can reach to 50 MW/m^2 and the thermal energy conversion by 40%.[5]

Tritium (T) inventory in the vacuum vessel has been identified as one of the most critical issues in the study of plasma wall interaction (PWI).[6] Safety limits for tritium must be less than 1 kg and administrative limits for tritium must be less than 700 g in ITER,[7] which is related to the economic and safety of fusion reactors. However, the permeation and retention behaviors of hydrogen isotopes (deuterium and tritium) in plasma-facing components (PFCs) make tritium self-sustaining severer. Hence the design of a fusion reactor requires a comprehensive and systematic understanding of the hydrogen isotopes recycling and retention in PFCs during operation.[8] Generally, hydrogen isotopes exist in the gaseous state and plasma state in fusion reactors. Therefore, its transport properties in PFCs should be considered from two different permeation approaches: one is gas-driven permeation (GDP), and the other is plasma-driven permeation (PDP).[9] Particularly for divertor plasma detachment,[10,11] the plasma in the divertor area combines into neutral particles, and the surface of the divertor target is covered by the neutral gas for plasma. In this process, both GDP and PDP may occur on the surface of the divertor.

In previous relavent studies, hydrogen isotope permeation through the solid metal membrane or liquid metal was studied separately. Zhou *et al.*[9,12] studied GDP and PDP through a reduced activation solid F82H membrane. The PDP of hydrogen isotopes in liquid metals such as Ga, Li, and GaInSn was discussed by Bi *et al.*,[13] and Bi and Hirooka.[14–16] A mesh sheet was firstly proposed to hold a liquid metal in their work. It was confirmed that PDP is the surface recombination-limited regime for liquid Li, and is diffusion-limited for liquid Ga and GaInSn. So far, the GDP and PDP of single liquid metal or solid metal have been mainly studied, and few studies of the double-layer permeation structure of liquid metals held on a solid metal membrane have been conducted. In the fusion device, liquid metals used as plasma-facing materials are cov-

†Corresponding author. E-mail: zbye@scu.edu.cn
‡Corresponding author. E-mail: gfujun@scu.edu.cn

© 2023 Chinese Physical Society and IOP Publishing Ltd

ered on solid metals, hence the study of the hydrogen permeation through the double-layer permeation structure composed of liquid metal and solid metal is important and necessary for future practical application in the fusion device.

In this work, the double-layer permeation structure of liquid GaInSn held on a solid α-Fe membrane is employed. The relationships of the hydrogen permeation flux, respectively, with temperature, hydrogen pressure, plasma density, and thickness of liquid metal are studied in the GDP/PDP experiment. And the permeation parameters such as diffusivity, Sieverts' constant, permeability, and surface recombination coefficient of hydrogen atoms are discussed.

2. Experimental details

The permeation facility as shown in Fig. 1 has been built for studying hydrogen permeation behaviors. It had two chambers. The left chamber in Fig. 1 was used to study the hydrogen transport in flowing liquid metals driven by a liquid metal loop in future work. The right chamber was used to study permeation behaviors in static liquid metals in this work. The volume of each chamber was $\sim$ 5969 cm^3, and either of the chambers could be used for PDP experiment and GDP experiment. The upper parts of both chambers could be pumped in H_2/D_2 for GDP experiments, and could be used as a plasma source for the PDP experiments as the inductively coupled plasma (ICP) ion source was installed. The low chambers were connected with a quadrupole mass spectrometer (QMS) to detect H-permeation flux by the change in H^+/H_2^+ ion current. The QMS (Pfeiffer Vacuum, QMG250) needed to work under ultra-high vacuum condition ($< 10^{-4}$ Pa). The QMSs were calibrated by an H_2 standard leak to obtain quantitative data.

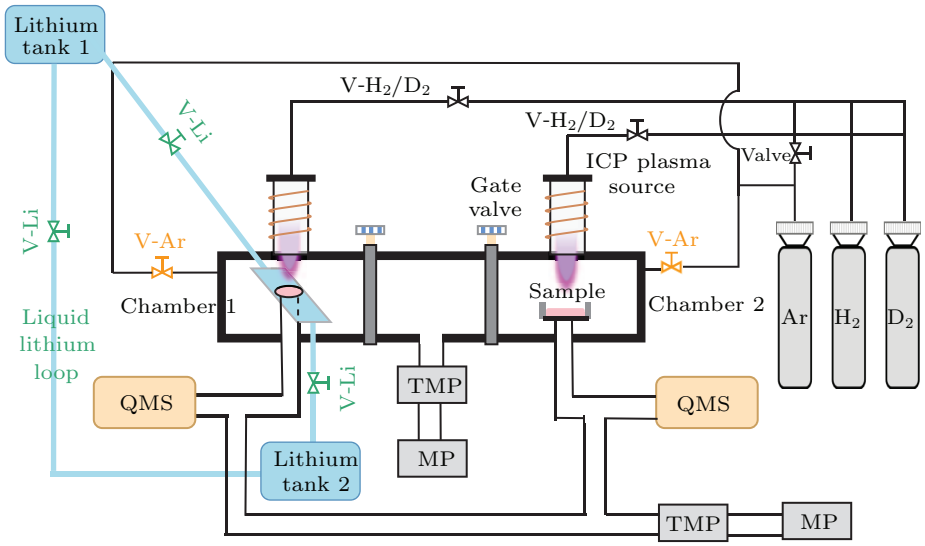


Fig. 1. Schematic diagram of permeation facility, TMP: turbo molecular pump, MP: mechanical pump, QMS: quadrupole mass spectrometer.

GaInSn is a low-temperature liquid metal alloy, which is compatible to a variety of metals within a wide temperature range.[13] Hence it was considered as a good modeling material to study the properties of liquid metals. The composition of liquid GaInSn selected in this experiment was 67% gallium, 20.5% indium, and 12.5% tin, and its melting point was 10.5 °C. Its other physical properties are shown in Table 1.

Table 1. Properties of liquid GaInSn.

Melting point (°C)	Boiling point (°C)	Density (kg·m^{-3})	Viscosity (m^2·s^{-1})	Conductivity (1 Ω·m^{-1})	Surface tension (N·m^{-1})
10.5	> 1300	6360	2.98×10^{-7}	3.1×10^{-6}	0.533

A schematic diagram of the working permeation model is shown in Fig. 2. Liquid GaInSn was held on an α-Fe membrane. Comparing with Al, Ni, Pt, and Cu, the diffusivities of hydrogen isotopes of α-Fe are higher,[14,15] and α-Fe has excellent thermal conductivity and high temperature mechanical properties. The container with a diameter of 20.5 mm and a height of 10 mm was composed of an α-Fe membrane and flange cover as shown in Fig. 2. The Fe membrane used in this work had a purity of 99.95 %, a diameter of 30.5 mm, and a thickness of 0.3 mm. Installation of two silver-plated inner opening spring enhanced C-rings under the Fe membrane, ensured that the top chamber and the low chamber are insulated from each other and maintain the ultrahigh vacuum. The size of C-rings was OD 30 mm×2.4 mm. The sample is heated in the device by a resistance wire circled below the Fe membrane. In the experiment, the surface temperature of the Fe membrane and the liquid GaInSn were measured by the thermocouple clamped on the flange as shown in Figs. 2 and 3.

Chamber 2 is divided into the top chamber and low chamber by the Fe membrane as shown in Fig. 2. The background vacuum degree of the top chamber was $\sim 10^{-4}$ Pa. By means of improving flanges structure, heating system and

sample sealing structure, as well as baking continuously the low chamber more than 24 hours at 300 K, the low chamber background vacuum degree was maintained at 10^{-5} Pa–10^{-6} Pa. As the experimental temperature increased gradually, there was no obvious change in the background vacuum degree of the low chamber. In addition, the change in temperature had no significant effect on the sealing of samples. The permeation data in this paper were obtained by subtracting the low chamber background partial pressure from the mass spectrometer partial pressure data obtained after permeation.

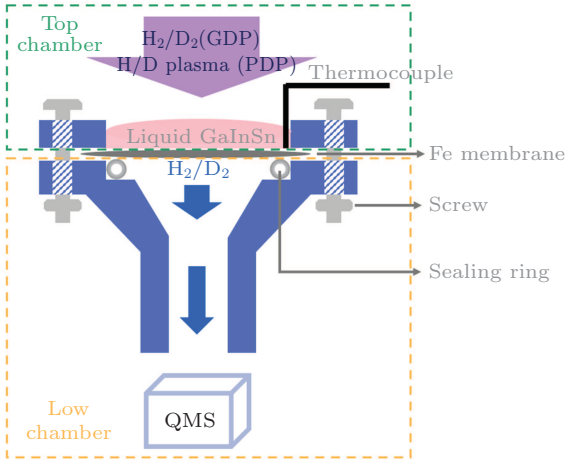


Fig. 2. Schematic diagram of working permeation model in chamber 2.

Liquid GaInSn was added at room temperature. At this temperature, the oxidation of liquid GaInSn was slow. At the beginning of the experiments, the sample temperature was raised to 673 K and allowed to stands for 10 min, so that the hydrogen and oxygen adsorbed by samples were degased from the environment. The oxide layer on the liquid metal surface was roughly scraped manually and completely removed by the bombardment of the liquid metal surface with argon plasma. Photographs of GaInSn with different thickness are shown in Fig. 3.

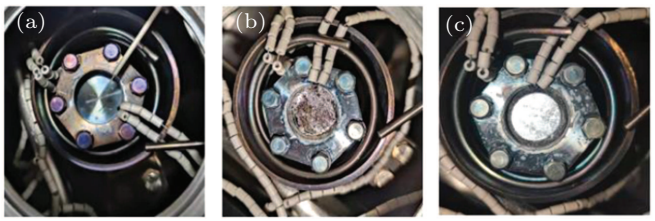


Fig. 3. Diagrams of samples of (a) Fe membrane, (b) 0.2-mm-thick GaInSn/Fe, and (c) 2-mm-thick GaInSn/Fe.

In the experiment of GDP, the pressure range of hydrogen pumped into the top chamber was adjusted to 4 Pa–400 Pa, and the experimental temperature range was adjusted to 573 K–693 K. In the experiment of PDP, hydrogen pressure for plasma production was 0.1 Pa. An ICP ion source was used to produce steady hydrogen plasma. The plasma flow linearly came downward and interacted with the liquid metal, as shown in Fig. 1. Plasma parameters could be measured by a movable Langmuir probe, where the electron temperature was ~ 8 eV, the plasma density was on the order of 10^9 cm^{-3}, and the plasma bombardment flux was on the order of 10^{15} H·cm^{-2}·s^{-1}.

3. Results and discussion

The hydrogen permeation behavior through liquid metal held on a solid metal membrane is studied by evaluating the hydrogen permeation flux, diffusivity, Sieverts' constant, permeability, and the surface recombination coefficient. In addition, the effects of various environmental factors on the hydrogen permeation behavior with different permeation approaches (GDP and PDP), such as temperature, hydrogen pressure, and thickness of liquid GaInSn are revealed.

3.1. Permeation and diffusion model

It is essential to establish a reasonable permeation model for studying hydrogen permeation. The GDP and PDP processes are complex physical and chemical processes as shown in Fig. 4. In the GDP process, the hydrogen molecules on the top surface are converted into hydrogen atoms through adsorption and dissociation. Part of the cracked hydrogen atoms are compounded again to form hydrogen molecules that escape from the surface. The remaining hydrogen atoms dissolve and diffuse in the metal medium, and are compounded into hydrogen on the low surface to permeate into the low chamber. In the process of PDP,[16] part of the hydrogen atoms and ions striking the surface are directly scattered back to the plasma. The number of particles returning rapidly to the plasma depends on the incident energy of the incoming particle and the type of material.[8] The ions are trapped in the implant zone in the form of hydrogen atoms. The implant zone is composed of various defects. In the extreme case of low hydrogen solubility in the implanted material, the recombination of hydrogen atoms may occur to form hydrogen escaping from the top surface. Hydrogen atoms that are not captured by the implant zone will continue to diffuse in the metal medium and compound on the low surface to form hydrogen escape.

Since the permeation model used in this work is composed of Fe membrane and liquid GaInSn, the activation energy values of various reactions of hydrogen atoms in the permeation process are sorted out as shown in Table 2. Hydrogen is hard to adsorb and dissociate on gallium and indium. And all the adsorption sites of tin have positive energy relative to H_2, that is, the dissociation of these is completely unfavorable.[17,18] Additionally, owing to the relatively low binding energy of hydrogen on gallium and indium, it can be expected that the dissociation of hydrogen on liquid GaInSn has an obvious energy barrier, leading the dissociation rate to decrease.[19]

Table 2. The H adsorption energy ($-\Delta E_{ads}$) and H dissociation energy ($-\Delta E_{dis}$) of metal atoms.

Atom species	Adsorption energy $-\Delta E_{ads}$ (eV)	Dissociation energy $-\Delta E_{dis}$ (eV)
α-Fe (Fe110)	~ 0.45[20]	~ 0.58[20]
Gallium	~ 1.73[21,22]	~ 0.1[21,23]
Indium	~ 2[21,22]	~ 0.167[21,23]

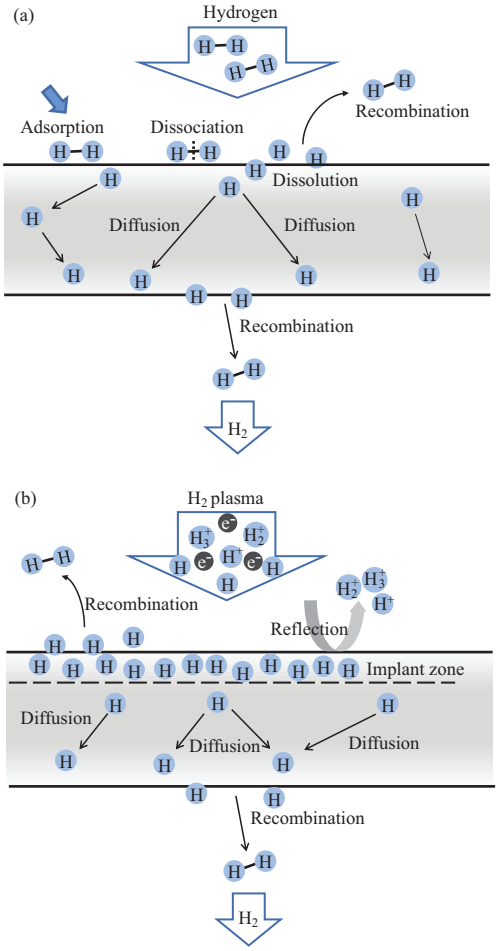


Fig. 4. Micro processes of (a) GDP and (b) PDP.

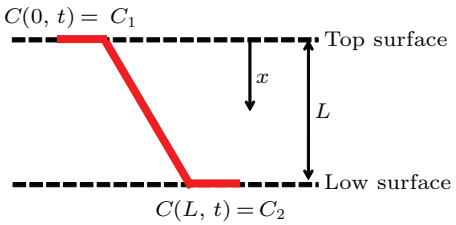


Fig. 5. Diffusion model.

A simple diffusion model can be described as shown in Fig. 5. Its diffusion equation can be expressed by Fick's second law[24]

$$\frac{\partial C}{\partial t} = D\frac{\partial^2 C}{\partial x^2}, \tag{1}$$

where C is the concentration of hydrogen atoms, D is the diffusivity, and L is the thickness.

The boundary conditions are

$$C(0,t) = C_1 = S\sqrt{p_1}, \tag{2}$$

$$C(L,t) = C_2 = S\sqrt{p_2}, \tag{3}$$

$$C(x,0) = 0, \quad 0 < x < L, \tag{4}$$

where S is the Sieverts' constant, p_1 and p_2 are the hydrogen pressures on the top surface and low surface, respectively. The solution to the equation is as follows:

$$C(x,t) = (C_1 - C_2)\left\{1 - \frac{x}{L} - \frac{2}{\pi}\sum_{n=1}^{\infty}\frac{1}{n}\sin\left(\frac{n\pi x}{L}\right) \times \exp(-Dn^2\pi^2 t/L^2)\right\}. \tag{5}$$

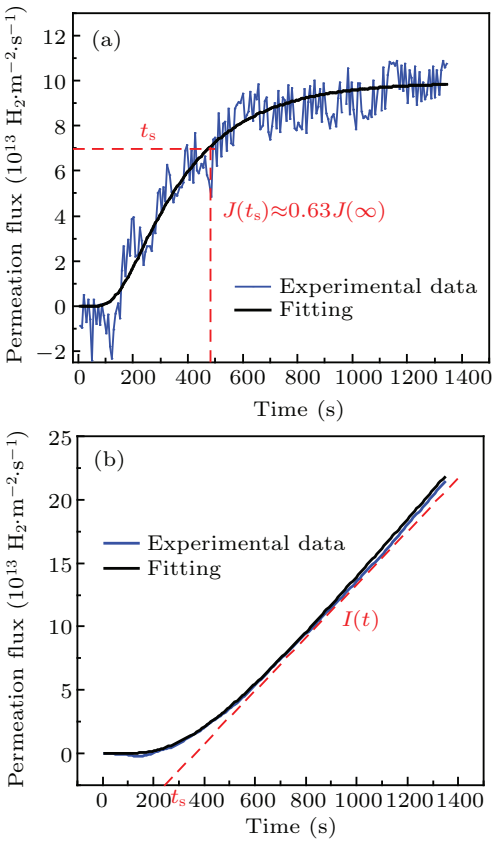


Fig. 6. (a) Fitting transient GDP flux curve and (b) GDP flux curve after time integration.

According to Fick' first law[24]

$$J = -D\frac{\partial C}{\partial x}, \tag{6}$$

where J is the permeation flux, so the permeation flux of the low surface can be expressed as[25]

$$J(L,t) = -D\left(\frac{\partial C}{\partial x}\right)\Big|_{x=L} = \frac{DS(\sqrt{p_1} - \sqrt{p_2})}{L} \times \left\{1 + 2\sum_{n=1}^{\infty}(-1)^n \exp(-Dn^2\pi^2 t/L^2)\right\}. \tag{7}$$

The integrated permeation flux on the low surface can be given by

$$\phi(t) = \int_0^t J(L,t)\,\mathrm{d}x$$

$$= \frac{D(C_1 - C_2)}{L}\left(t - \frac{L^2}{6D}\right) - \frac{2L(C_1 - C_2)}{\pi^2} \times \sum_{n=1}^{\infty} \frac{(-1)^n}{n^2} \exp(-Dn^2\pi^2 t/L^2). \quad (8)$$

It can be seen from Eq. (8) that when time tends to infinity, the curve of $\phi(t)$ will be close to $I(t)$ and the expression of $I(t)$ is as follows:[25]

$$I(t) = \frac{DC_0}{L}\left(x - \frac{L^2}{6D}\right). \quad (9)$$

The intersection point of the $I(t)$ curve and the time axis is lag time t_s (shown in Fig. 6(b)), $J(t_s) = 0.63J(\infty)$, so D satisfies

$$t_s = \frac{L^2}{6D}. \quad (10)$$

3.2. Hydrogen gas-driven permeation

The output data of QMS is ion current I, which can be converted into the gas pressure through

$$K = \frac{I}{p'}, \quad (11)$$

where p' is the partial pressure of the gas, and K is the sensitivity of QMS. In this work, $K = 9.66 \times 10^{-6}$ (A·Pa^{-1}).

The extraction rate of the vacuum system in the low chamber $S' = 0.7$. And the permeation rate Q can be calculated from[26]

$$Q = (p_0 - p'') \cdot S', \quad (12)$$

where p'' is the pressure after permeation and S' is the extraction rate of the low chamber. The equation for converting permeation rate Q into permeation flux f (molecule·s^{-1}) can be expressed as

$$f = Q/(1.013 \times 10^5 \times 0.0224) \times \frac{T}{T_{0\,^\circ\mathrm{C}}} \times N_\mathrm{A}, \quad (13)$$

where T is the current temperature, and $N_\mathrm{A} = 6.02214076 \times 10^{23}$ mol^{-1} is Avogadro constant.

3.2.1. Fe membrane

In order to study the permeation model of liquid metal held on a solid metal membrane, the hydrogen permeation behavior in the Fe membrane is discussed first.

Here, the steady-state hydrogen GDP flux through a 0.3-mm-thick Fe membrane in a temperature range of 580 K–670 K is shown in Fig. 7. Equation (7) is used to fit the permeation curves. This fitting method can achieve the satisfactory results in the temperature range selected in this experiment. In Fig. 7, t_1 represents the reaction time of hydrogen permeation detected by the QMS from the top chamber to the low chamber, and t_2 denotes the time in which the permeation curve reaches the steady-state. Taking the permeation curve at 579 K in Fig. 7 for example, when the time is less than t_1, the permeation flux is extremely small, and the hydrogen in the top chamber hardly permeates into the lower chamber. When the time reaches t_1 ($\sim$ 40 s), the permeation curve begins to rise continuously. After continuously proceeding for t_2 (20 s–25 s), the permeation curve maintains stability. Figure 7 reveals that as the temperature rises from 579 K to 664 K, t_2 shows slight degradation, and hydrogen permeation flux increases from 7.7×10^{13} H_2·cm^{-2}·s^{-1} to 2.5×10^{14} H_2·cm^{-2}·s^{-1}.

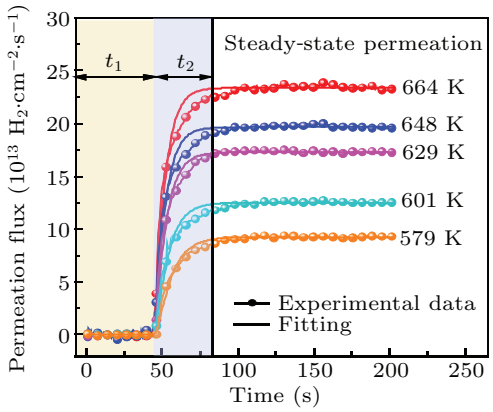


Fig. 7. Time evolutions of hydrogen permeation flux through Fe membrane for different temperatures, with hydrogen pressure kept at 4 Pa for all tests.

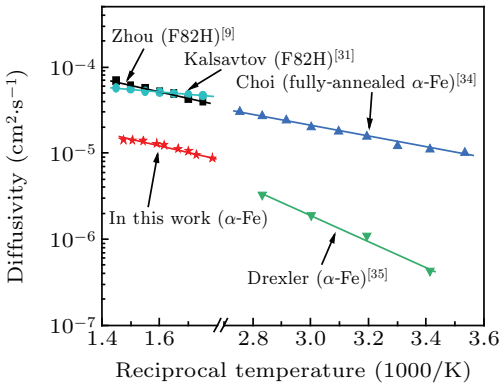


Fig. 8. Plots of diffusivity *versus* reciprocal temperature of hydrogen atoms in Fe membrane for different temperatures.

Substituting Eq. (10) with the time evolutions of hydrogen permeation flux data into Fig. 7, the diffusivity of the hydrogen atoms in the Fe membrane is shown in Fig. 8. The variation of diffusivity conforms to the Arrhenius equation and is shown as follows:

$$D = D_0 \exp\left[-\frac{\Delta E_\mathrm{d}}{K_\mathrm{B}T}\right], \quad (14)$$

where D_0 is the diffusion pre-exponential factor, ΔE_d denotes the diffusion activation energy, and K_B represents the Boltzmann constant. The D of Fe membrane used in this work can be obtained to be

$$D_\mathrm{Fe} = 1.7486 \times 10^{-8} \exp\left[-\frac{0.1431\ (\mathrm{eV})}{K_\mathrm{B}T}\right]. \quad (15)$$

As the temperature of the Fe membrane increases from 580 K to 670 K, the diffusivity of hydrogen increases from 8.7×10^{-6} cm^{-2}·s^{-1} to 1.5×10^{-5} cm^{-2}·s^{-1}. The diffusivity

of the Fe membrane obtained here is less than the diffusivity of hydrogen through F82H measured by Zhou *et al.*[9] and Kulsavtov *et al.*[27] The diffusion activation energy of F82H is ~ 0.145 eV,[12,27–29] which is similar to the measured diffusion activation energy of the Fe membrane. The diffusion path of hydrogen atoms inside the material may lead to different diffusivities of Fe and F82H. In a temperature range of 283 K–373 K, the diffusivity of hydrogen through completely annealing α-Fe is 1×10^{-6} $\mathrm{cm^{-2}\cdot s^{-1}}$–$3\times10^{-6}$ $\mathrm{cm^{-2}\cdot s^{-1}}$,[30] which is larger than that of hydrogen through unannealing α-Fe. Moreover, the diffusivity through α-Fe is obtained to be 0.43×10^{-6} $\mathrm{cm^{-2}\cdot s^{-1}}$–$3.3\times10^{-6}$ $\mathrm{cm^{-2}\cdot s^{-1}}$ in a range of 293 K–353 K,[31] which is basically in agreement with the linear variation by comparing our data in a range from 579 K to 664 K.

The hydrogen permeation flux and diffusivity are strongly dependent on temperature. As shown in Eq. (7), the permeation flux of hydrogen through the Fe membrane is directly proportional to the diffusivity, and owing to the diffusivity being positively associated with temperature as shown in Fig. 8, the rising of temperature will cause the increase of hydrogen permeation flux.

The steady-state hydrogen GDP flux through the Fe membrane at 648 K is obtained in a pressure range of 50 Pa–450 Pa as shown in Fig. 9. The t_3 represents the time in which the permeation curve reaches the steady-state in Fig. 9. The increase of hydrogen molecular density leads to the saturated permeation flux to increase from 9.3×10^{14} $\mathrm{H_2\cdot cm^{-2}\cdot s^{-1}}$ to 2.4×10^{15} $\mathrm{H_2\cdot cm^{-2}\cdot s^{-1}}$. Besides, the permeation curve reaches the steady-state quickly. And the values of t_3 at different pressures are almost equal because the experimental temperature is the same. The fitting curves in Fig. 7 (4 Pa) and Fig. 9 ($\geq$ 50 Pa) are compared, and it reveals that permeation flux under high pressure fits well with the experimental data.

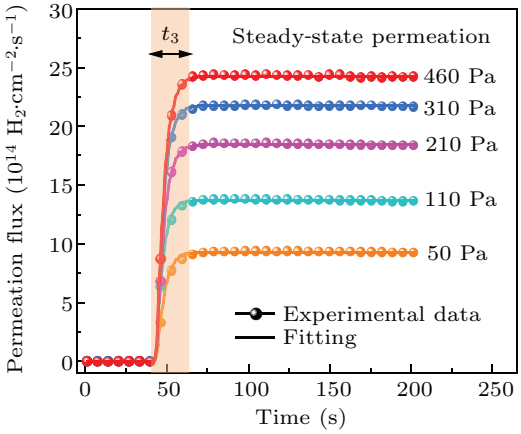


Fig. 9. Time evolutions of hydrogen GDP permeation flux through Fe membrane for different pressures, with temperature kept at 648 K for all tests.

The effects of temperature and pressure on the permeation flux are summarized and compared in the temperature range of 580 K–670 K and the hydrogen pressure range of 50 Pa–450 Pa as shown in Fig. 10. The effect of hydrogen pressure on permeation flux takes the main advantage within the test scope of this work.

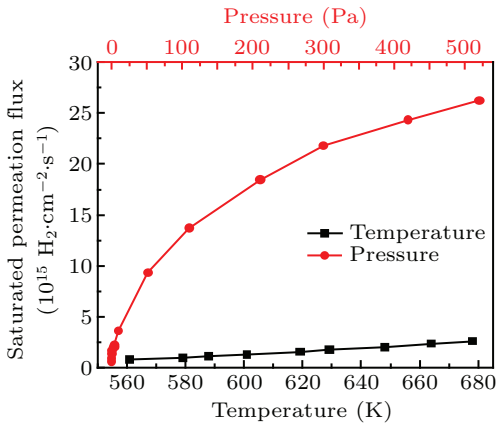


Fig. 10. Curves of hydrogen saturated GDP flux through Fe membrane versus temperature and pressure, respectively.

The hydrogen through the Fe membrane meets the diffusion-limited regime, and the differences in the membrane surface composition seems to have no measurable effect on permeability.[32,33] The steady-state diffusion-limited GDP flux of the Fe membrane can be given as follows:[9]

$$J(\infty) = \frac{D\cdot S\cdot\sqrt{p_\mathrm{s}}}{L} = \frac{P\cdot\sqrt{p_\mathrm{s}}}{L}, \tag{16}$$

where p_s is the surface pressure of the Fe membrane, L is the thickness of the Fe membrane, and P is the permeability. It can also be seen from Fig. 10 that the saturated permeation flux and the hydrogen pressure satisfy $J \propto \sqrt{p_\mathrm{s}}$. With the known parameters above, relationship of P and S with temperature in this experiment is given in Fig. 11.

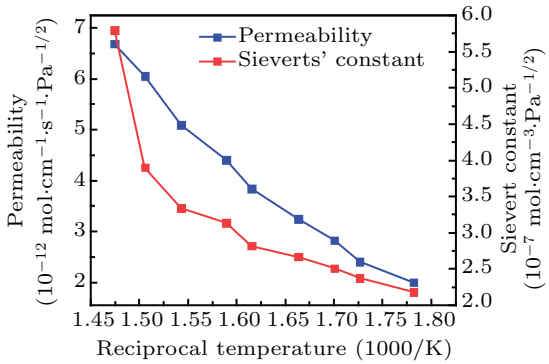


Fig. 11. The P and S *versus* reciprocal temperature in this experiment.

The P and S varying with temperature also basically conform to the Arrhenius equation, and specifically, are expressed as

$$S = S_0 \exp\left[-\frac{\Delta H}{K_\mathrm{B}T}\right], \tag{17}$$

$$P = P_0 \exp\left[-\frac{\Delta E_\mathrm{P}}{K_\mathrm{B}T}\right], \tag{18}$$

where S_0 is the dissolving pre-exponential factor, ΔH represents the heat of solutio, P_0 denotes the pre-permeability factor, ΔE_P refers to the osmotic activation energy. The P and S of Fe membrane used in this work can be given as follows:

$$S_{Fe} = 2.276 \times 10^{-5} \exp\left[-\frac{0.2289\ (eV)}{K_B T}\right], \quad (19)$$

$$P_{Fe} = 2.367 \times 10^{-9} \exp\left[-\frac{0.3421\ (eV)}{K_B T}\right]. \quad (20)$$

3.2.2. GaInSn/Fe membrane

As indicated above, hydrogen permeation behavior in the Fe membrane is studied. Next, the study of the hydrogen GDP behavior through GaInSn/Fe is mainly carried out from two aspects: (i) comparison of hydrogen GDP behavior between Fe membrane and GaInSn/Fe; (ii) the effect of GaInSn thickness on the GDP behavior of GaInSn/Fe.

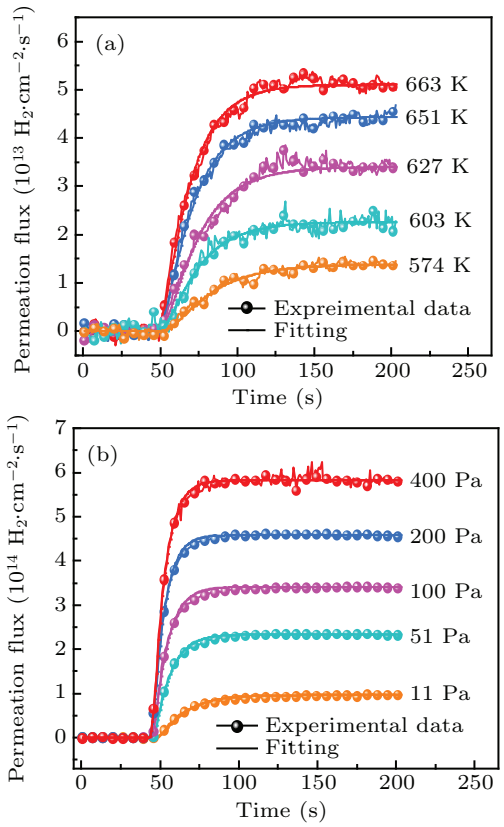


Fig. 12. Time evolutions of hydrogen GDP flux through 0.2-mm-thick GaInSn/Fe for (a) different temperatures, with hydrogen pressure kept at 4 Pa for all tests, and (b) different pressures, with temperature kept at 648 K.

Firstly, the permeation behaviors of hydrogen through the Fe membrane and GaInSn/Fe are compared under almost the same experimental conditions. Under the experimental H_2 pressure of 4Pa and temperature range of 574 K–663 K, the permeation flux of hydrogen through the 0.2-mm-thick GaInSn/Fe is shown in Fig. 12(a). It can be seen that the permeation law of 0.2-mm-thick GaInSn/Fe is similar to that of the Fe membrane. And the permeation flux of hydrogen through 0.2-mm-thick GaInSn/Fe increases from 1.38×10^{13} H_2·cm^{-2}·s^{-1} to 5.11×10^{13} H_2·cm^{-2}·s^{-1}. Under the experimental temperature of 648 K and the H_2 pressure range of 50 Pa–450 Pa, the permeation flux of hydrogen through 0.2-mm-thick GaInSn/Fe is shown in Fig. 12(b). It shows that the permeation flux of hydrogen through 0.2-mm-thick GaInSn/Fe grows from 2.3×10^{14} H_2·cm^{-2}·s^{-1} to 6.5×10^{14} H_2·cm^{-2}·s^{-1}. Obviously, the permeation flux of 0.2-mm-thick GaInSn/Fe is far below compared with that of the Fe membrane. A possible reason for that is the thickness of the permeation model increases after adding liquid GaInSn. And the permeation flux is inversely proportional to the thickness of the model as shown in Eq. (7). Another obvious phenomenon is the permeation flux curve of hydrogen through GaInSn/Fe fluctuates greatly due to the natural convection of liquid metals.[34] Moreover, The time for hydrogen permeation through Fe membrane to reach the steady-state is 80 s–100 s less than that of 0.2-mm-thick GaInSn/Fe at the same temperature. The reasons for GaInSn/Fe permeation time growth will be discussed later.

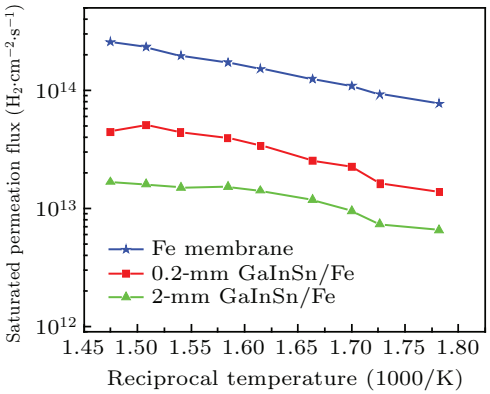


Fig. 13. Comparison of saturated permeation flux between Fe membrane and GaInSn/Fe for different temperatures.

For a further look into the hydrogen permeation in GaInSn/Fe, two different thickness values of GaInSn, 0.2 mm and 2 mm, are studied in Fig. 13. Corresponding photographs of GaInSn with different thickness values are shown in Fig. 3. The results show that the permeation flux of the Fe membrane is higher obviously than that of the GaInSn/Fe under the same experimental condition. Furthermore, the 0.2-mm-thick GaInSn/Fe represents significantly enlarged permeation flux in comparison with the 2-mm-thick GaInSn/Fe. Notably, the thickness of GaInSn is inversely proportional to the hydrogen permeation flux. Thus, hydrogen through GaInSn/Fe is a typical diffusion-limited permeation. In the diffusion-limited regime, the permeation rate mainly depends on the diffusivity. Despite this, it can be seen from Table 2 that the dissociation of hydrogen on liquid GaInSn has an obvious energy barrier that will reduce the dissociation rate. The energy barrier causes the permeation rate to be limited not only by the diffusivity but also by the dissociation rate,[19] which prolongs the permeation time. This conclusion can be used to explain that the

permeation time of GaInSn/Fe is longer than that of the Fe membrane as shown in Fig. 12(a).

The D of hydrogen atoms in GaInSn is much larger than that of hydrogen atoms in the Fe membrane as shown in Fig. 14(a). The D of 0.2-mm-thick GaInSn/Fe is about 1×10^{-5} cm^{-2}·s^{-1}–2×10^{-5} cm^{-2}·s^{-1}, which is less than that of 2-mm-thick GaInSn/Fe(about 1×10^{-4} cm^{-2}·s^{-1}–3×10^{-4} cm^{-2}·s^{-1}), which once again confirms that the hydrogen through GaInSn/Fe meets the diffusion-limited regime. Moreover, the D of hydrogen in 0.2-mm-thick GaInSn/Fe is almost the same as that of hydrogen in Fe membrane, which can be attributed to the thin GaInSn with a thickness of 0.2 mm, and the diffusivity is mainly dominated by Fe.

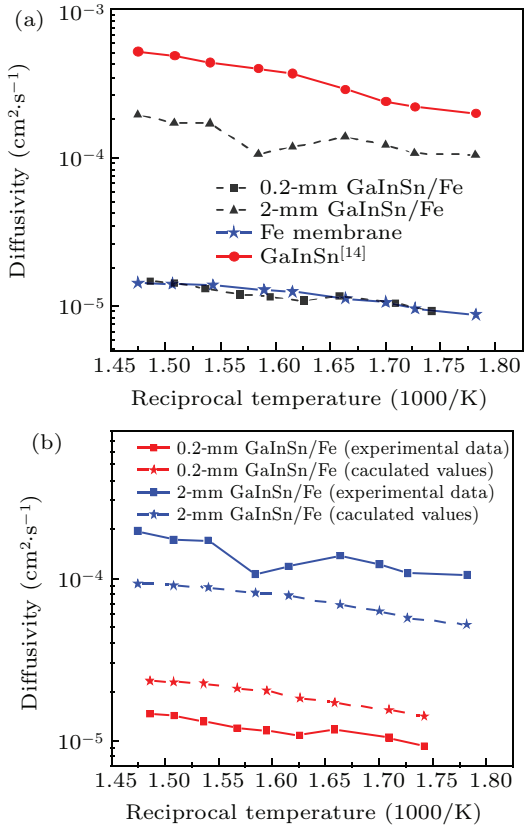


Fig. 14. (a) Curves of diffusivity D varying with reciprical temperature of Fe membrane and GaInSn/Fe and (b) comparison between measured data D value and calculated D values from multilayer theory.

To further investigate the hydrogen permeation in GaInSn/Fe, a multi-layer permeation model is employed.[35] The total diffusivity of multi-layer permeation film is related to the thickness of each layer, which can be expressed as

$$\frac{d_{\rm all}}{D_{\rm all}}=\frac{d_{\rm Fe}}{D_{\rm Fe}}+\frac{d_{\rm GaInSn}}{D_{\rm GaInSn}}, \tag{21}$$

where $d_{\rm Fe}$, $d_{\rm GaInSn}$, and $d_{\rm all}$ represent the thickness of Fe membrane, liquid GaInSn, and the entire multi-layer respectively; $D_{\rm Fe}$, $D_{\rm GaInSn}$, and $D_{\rm all}$ denote the hydrogen diffusivity of Fe membrane, liquid GaInSn, and the entire multi-layer respectively. The comparison between experimental data and calculated values from multi-layer theory is shown in Fig. 14(b). The experimental values are in good agreement with the calculated values, which can prove that the multi-layer theory is applicable to the GaInSn/Fe permeation model. However, the small error between the theoretical values and the experimental data may be due to the interface effect between the Fe membrane and liquid GaInSn.

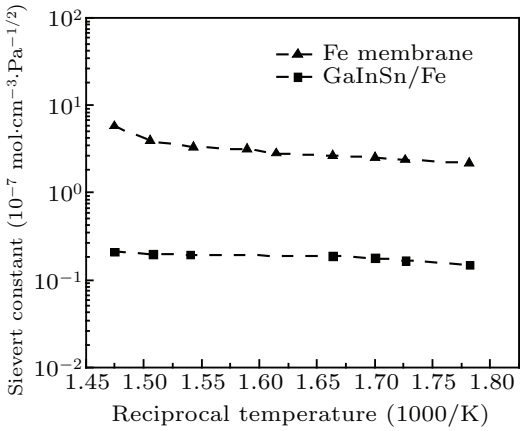


Fig. 15. Curve of Sievert constant S *versus* reciprocal temperature of Fe membrane and GaInSn/Fe.

Using Eq. (16), the value of S of hydrogen atoms in Fe membrane and GaInSn/Fe are obtained in Fig. 15. The S, as a material property of liquid metal, is generally used only under the boundary conditions of the top surface of liquid metal and does not change with thickness. The value of S of Fe membrane and GaInSn/Fe grow with the temperature increasing. The S value of GaInSn/Fe is about 2 mol·cm^{-3}·Pa$^{-1/2}$–3×10^{-8} mol·cm^{-3}·Pa$^{-1/2}$, and that of Fe is about 3×10^{-8} mol·cm^{-3}·Pa$^{-1/2}$–8×10^{-8} mol·cm^{-3}·Pa$^{-1/2}$. Clearly, the decrease in the solubility of hydrogen atoms in GaInSn/Fe further explains the reason that the permeation flux of hydrogen through GaInSn/Fe membrane is smaller than that through the Fe membrane.

In summary, D and P of 0.2-mm-thick GaInSn/Fe and 2-mm-thick GaInSn/Fe can be obtained as follows.

For 0.2-mm-thick GaInSn/Fe,

$$D=1.5413\times10^{-8}\exp\left[-\frac{0.1378\ ({\rm eV})}{K_{\rm B}T}\right], \tag{22}$$

$$P=5.3290\times10^{-9}\exp\left[-\frac{0.4480\ ({\rm eV})}{K_{\rm B}T}\right]; \tag{23}$$

for 2-mm-thick GaInSn/Fe,

$$D=2.7676\times10^{-7}\exp\left[-\frac{0.1610\ ({\rm eV})}{K_{\rm B}T}\right], \tag{24}$$

$$P=3.7551\times10^{-10}\exp\left[-\frac{0.2618\ ({\rm eV})}{K_{\rm B}T}\right]. \tag{25}$$

3.3. Hydrogen plasma-driven permeation

The hydrogen plasma bombards the surface of the PFCs in the fusion reactor, the PDP occurs on the plasma-facing side of the PFCs. The microscopic physical process of PDP is illustrated in Fig. 4(b). The hydrogen atoms are easier to capture

on the surface of liquid metal for PDP than for GDP, and thus inducing the hydrogen atoms retention to be enhanced.[8] The prominent discrepancy between GDP and PDP is the interaction between hydrogen/hydrogen plasma with the top surface of liquid metal. Hence the surface recombination coefficient (Kr), as a crucial parameter in PDP, needs studying.

In the PDP experiments, the electromagnetic field is produced by a high-frequency current through an induction coil. The H_2 is ionized into H plasma, which causes PDP, but a large number of unionized hydrogen atoms will cause GDP at the same time. As a result, it is vital to choose the pressure of H_2 and ignore the influence of GDP on PDP as much as possible. Figure 16 shows the permeation fluxes of hydrogen through 0.2-mm-thick GaInSn/Fe in GDP and PDP experiment under the hydrogen pressure is 10 Pa, 5 Pa, 1 Pa, and 0.1 Pa, respectively. It reveals the corresponding GDP permeation fluxes are 1.11×10^{14} $H_2\cdot cm^{-2}\cdot s^{-1}$ (10 Pa), 7.30×10^{13} $H_2\cdot cm^{-2}\cdot s^{-1}$ (5 Pa), 6.80×10^{13} $H_2\cdot cm^{-2}\cdot s^{-1}$ (1 Pa), and 8.65×10^{12} $H_2\cdot cm^{-2}\cdot s^{-1}$ (0.1 Pa), and the corresponding PDP permeation fluxes in steady-state are 3.18×10^{14} $H_2\cdot cm^{-2}\cdot s^{-1}$ (10 Pa), 1.83×10^{14} $H_2\cdot cm^{-2}\cdot s^{-1}$ (5 Pa), 1.72×10^{14} $H_2\cdot cm^{-2}\cdot s^{-1}$ (1 Pa), and 1.57×10^{14} $H_2\cdot cm^{-2}\cdot s^{-1}$ (0.1 Pa). Obviously, the permeation flux of GDP relative to that of PDP is extremely difficult to ignore at the hydrogen pressures of 10 Pa, 5 Pa, and 1 Pa. It can be seen that the permeation flux of PDP is dominated under the H_2 pressure of 0.1 Pa. Therefore, the following PDP experiments are completed in the environment hydrogen pressure of 0.1 Pa in this work.

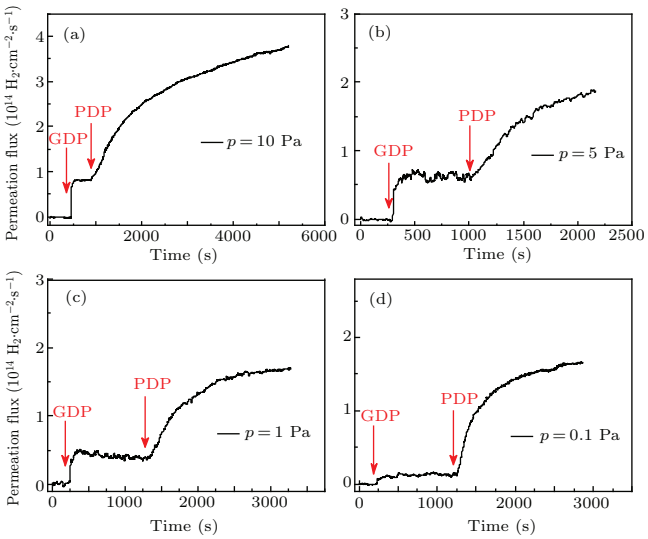


Fig. 16. Time-dependent hydrogen GDP and PDP permeation fluxes through 0.2-mm-thick GaInSn/Fe with the different pressures, with temperature kept at 673 K.

The permeation curves of GDP and PDP are compared in Fig. 17. With the experimental conditions of 0.1-Pa hydrogen pressure, the permeation flux of hydrogen is 1.64×10^{14} $H_2\cdot cm^{-2}\cdot s^{-1}$ in PDP and 6.29×10^{12} $H_2\cdot cm^{-2}\cdot s^{-1}$ in GDP. The GDP flux of hydrogen is 4.86×10^{13} $H_2\cdot cm^{-2}\cdot s^{-1}$ under the experimental hydrogen pressure of 4 Pa. Although the hydrogen pressure in the GDP experiment increases 40 times, the PDP permeation flux still occupies a major advantage. In addition, the time for reaching steady-state permeation is $\sim$ 200 s in the GDP experiment, and the time is $\sim$ 2000 s in the PDP experiment, which is far greater than the time for GDP. The cause of this phenomenon is not entirely clear and needs exploring in the future.

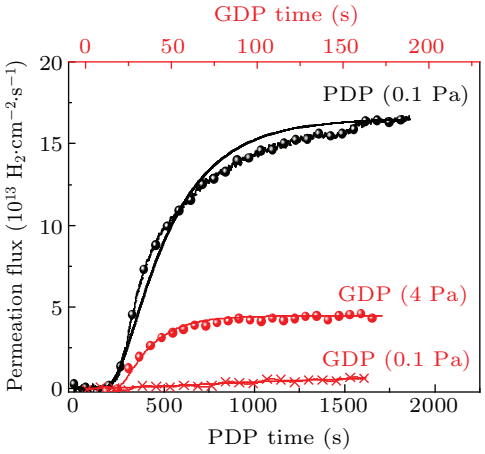


Fig. 17. Comparison of hydrogen permeation through 0.2-mm GaInSn/Fe between GDP and PDP at 693 K, with GDP hydrogen pressure being 0.1 Pa and 4 Pa, and PDP hydrogen pressure being 0.1 Pa.

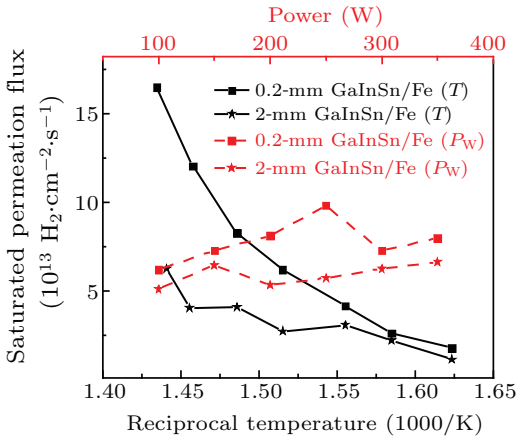


Fig. 18. Effects of temperature (in units of K) and ICP power (P_W) on steady-state hydrogen PDP saturated flux through 0.2-mm-thick GaInSn/Fe and 2-mm-thick GaInSn/Fe.

It is shown that hydrogen PDP flux is also strongly dependent on temperature as shown in Fig. 18. The plasma parameters corresponding to the ICP power supply are listed in Table 3. Although the plasma density increases with the augment of power supply, the changes of plasma parameters do not cause the hydrogen PDP flux to change significantly. The reason for that is the hydrogen atoms dissolved in the liquid metal have reached saturation even though the ICP power is 100 W, so even if more hydrogen plasmas bombard the surface of the liquid metal, the number of hydrogen atoms dissolved in the liquid metal will not change.

Table 3. Hydrogen plasma parameters in PDP process under hydrogen pressure 0.1 Pa.

Power (W)	T_e (eV)	n_e (10^8 cm^{-3})	Γ_i (10^{15} H·cm^{-2}·s^{-1})	Ionization rate (%)
100	7.467±0.092	6.236±0.173	1.205±0.04024	0.16
150	8.218±0.051	8.374±0.030	1.697±0.00664	0.22
200	8.779±0.036	11.82±0.046	2.477±0.00584	0.31
250	9.175±0.046	14.11±0.141	3.022±0.02897	0.37
300	9.240±0.046	16.29±0.018	3.501±0.00536	0.42
350	9.356±0.035	18.67±0.182	4.038±0.03692	0.48

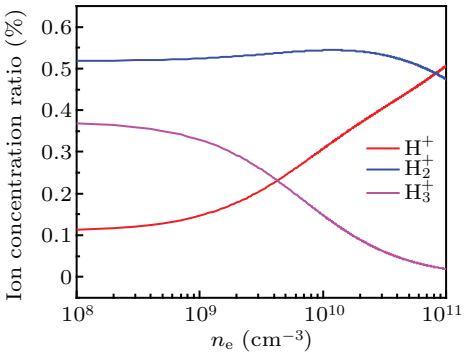


Fig. 19. Ions concentration ratios *versus* electron density of H_3^+, H_2^+, and H^+ ($T_e = 8$ eV).

The number of incident hydrogen ions has a great influence on the study of surface recombination coefficient in PDP experiments. In a hydrogen plasma, the concentrations of H_3^+, H_2^+, and H^+ are controlled by a series of homogeneous and multi-phase reactions.[36] The concentration ratios of H_3^+, H_2^+, and H^+ at different electron densities are obtained by solving the equilibrium equation of hydrogen atom and ion concentration kinetics,[37] as shown in Fig. 19. In general, the ion composition in hydrogen plasma is dominated by H_3^+, while H_2^+ may dominate under low pressure.[37] Apparently, H_2^+ dominates at an experimental hydrogen pressure of 0.1 Pa. In this work, the electron density can reach $\sim 10^9$ cm^{-3} and the electron temperature is 8 eV. Under this experimental condition, the ion concentration in hydrogen plasma is about 35% H_3^+, 50% H_2^+, and 15% H^+.

The incident hydrogen molecule and H^+ flux in the plasma are as follows:

$$\Gamma_{H_2} = \frac{p_{H_2}(t)}{\sqrt{2\pi m_{H_2} K_B T}}, \tag{26}$$

$$\Gamma_{H^+} \approx \frac{1}{2} n_e \sqrt{\frac{K_B T_e}{m_H}}, \tag{27}$$

$$\Gamma_{all} = \Gamma_{H^+} + 2\Gamma_{H_2}, \tag{28}$$

where m_{H_2} is the molecular weight of hydrogen, and m_H is the atomic weight of hydrogen. The total incident flux can be corrected by the ion concentration ratio (35% H_3^+, 50% H_2^+, and 15% H^+):

$$\begin{aligned}\Gamma'_{all} &= 0.35 \times 3\Gamma_{H_3^+} + 0.5 \times 2\Gamma_{H_2^+} \\ &\quad + 0.15\Gamma_{H^+} + 0.15 \times 0.5\Gamma_{H^0} + 2\Gamma_{H_2} \\ &= 2.275\Gamma_{H^+} + 2\Gamma_{H_2}. \end{aligned} \tag{29}$$

Among them, the flux of hydrogen molecules dominates in the incident flux. Whereas the compound sticking coefficient of hydrogen molecules is significantly smaller than that of ions in the hydrogen plasma.[38] Therefore, the effect of incident hydrogen atoms on the surface is ignored, and the total incident flux is $\Gamma'_{all} \approx 2.275\Gamma_{H^+} \approx 2.74 \times 10^{15}$ H·cm^{-2}·s^{-1}. As shown in Fig. 18, the hydrogen PDP flux decreases with the increase of liquid metal thickness, which can be speculated in such a way that the diffusion of hydrogen atoms in GaInSn/Fe in PDP meets the diffusion-limited condition. The PDP flux satisfies

$$J_+ = \frac{D}{L}\sqrt{\frac{J_0}{Kr}}, \tag{30}$$

where J_+ is the permeation flux, J_0 is the surface incident flux, and Kr is the surface recombination coefficient, as shown in Fig. 20.

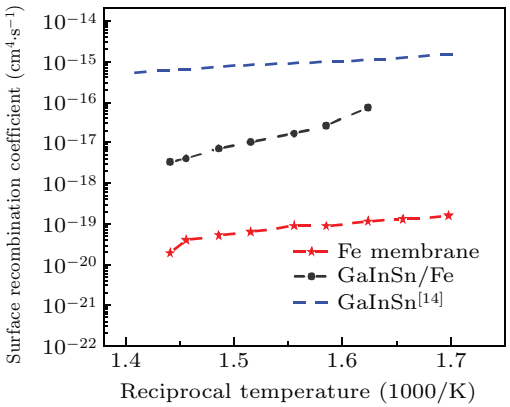


Fig. 20. Curves of Kr *versus* reciprocal temperature of Fe membrane and GaInSn/Fe.

From the results in Fig. 20, it can be obtained that the surface recombination coefficient (Kr) of all samples decreases with temperature rising. The permeation flux is closely related to Kr. The value of Kr of GaInSn/Fe, Fe membrane, and single liquid GaInSn are respectively 3×10^{-18} cm^4·s^{-1}–7×10^{-17} cm^4·s^{-1}, 2×10^{-20} cm^4·s^{-1}–1.5×10^{-19} cm^4·s^{-1}, and $\sim 1\times10^{-15}$ cm^4·s^{-1} under the temperature range of 579 K–664 K. It can be seen that the permeation flux of GaInSn/Fe is less than that of the Fe membrane in Fig. 13, while the Kr of GaInSn/Fe takes a greater advantage in Fig. 20.

This can indicate that the permeation flux is inversely proportional to Kr. The Kr is also a material property, which is similar to S. It is generally used only for the boundary condition of the top surface of liquid metal and does not change with thickness. The surface recombination occurs on the top surface of liquid GaInSn for GaInSn/Fe and single liquid GaInSn, whereas the Kr of GaInSn/Fe is less than that of single liquid GaInSn obtained by Bi and Hirooka.[39] The reason may be that the influence of the interface effect between the Fe membrane and the liquid metal affects the hydrogen permeation flux and diffusivity, resulting in the deviation of the Kr calculated from Eq. (30). In future work, equation (30) should be modified to minimize the influence of the interface effect in the double-layer permeation structure on the Kr.

4. Conclusions

The hydrogen permeation behaviors of GDP and PDP in GaInSn/Fe are systematically studied. The permeation flux, diffusivity, permeability, Sieverts' constant, and surface recombination coefficient are measured and calculated. From the experimental results, it can be concluded that GaInSn/Fe prolongs the permeation time and reduces the hydrogen permeation flux. Furthermore, the hydrogen permeation behavior through GaInSn/Fe is also in good agreement with the multilayer permeation theory. Furthermore, the experimental results show that the PDP flux is greater than the GDP flux. Whether the experiment is of GDP or PDP, the permeation flux of hydrogen is dependent on temperature and the thickness of GaInSn. In PDP experiment, the increase of hydrogen plasma density almost does not cause the hydrogen permeation flux to change, which may be explained by the dissolution saturation of hydrogen atoms in liquid metal. In both PDP and GDP experiments, hydrogen through GaInSn/Fe satisfies the diffusion-limited regime. The interfacial effect at the interface between liquid GaInSn and Fe membrane may have a crucial influence on the hydrogen permeation behavior in GaInSn/Fe, hence more experiments and modeling work are needed on the topic of the interface effect.

Acknowledgements

Project supported by the National Natural Science Foundation of China (Grant Nos. 11905151 and 11875198) and the National Key Research and Development Program of China (Grant No. 2022YFE03130000).

References

[1] Martin-Rojo A B, Oyarzabal E, Morgan T W and Tabarés F L 2017 *Fusion Eng. Des.* **117** 222
[2] Kugel H W, Allain J P, Bell M G, *et al*. 2012 *Fusion Eng. Des.* **87** 1724
[3] Hu J S, Zuo G Z, Ren J, *et al*. 2016 *Nucl. Fusion* **56** 046011
[4] Vertkov A, Luyblinski I, Evtikhin V, Mazzitelli G, Apicella M L, Lazarev V, Alekseyev A and Khomyakov S 2007 *Fusion Eng. Des.* **82** 1627
[5] Frazer D, Stergar E, Cionea C and Hosemann P 2014 *Energy Procedia* **49** 627
[6] Roth J, Tsitrone E, Loarer T, Philipps V, Brezinsek S, Loarte A, Counsell G F, Doerner R P, Schmid K, Ogorodnikova O V and Causey R A 2008 *Plasma Phys. Control. Fusion* **50** 103001
[7] Roth J, Tsitrone E, Loarte A, *et al*. 2009 *J. Nucl. Mater.* **390** 1
[8] Bi H 2017 *Hydrogen isotopes transport in liquid metals under steady state plasma bombardment*, Ph.D. dissertation (Department of Fusion Science School of Physical Sciences SOKENDAI (The Graduate University for Advanced Studies)) (in Japan)
[9] Zhou H, Hirooka Y, Ashikawa N, Muroga T and Sagara A 2014 *J. Nucl. Mater.* **455** 470
[10] Stangeby P C 2018 *Plasma Phys. Control. Fusion* **60** 044022
[11] Ohno N 2017 *Plasma Phys. Control. Fusion* **59** 034007
[12] Zhou H, Hirooka Y, Ashikawa N, Muroga T and Sagara A 2013 *Plasma and Fusion Research* **8** 2402065
[13] Bi H, Hirooka Y and Yagi J 2016 *Plasma and Fusion Research* **11** 2405026
[14] Bi H and Hirooka Y 2019 *IEEE Trans. Plasma Science* **47** 3009
[15] Bi H and Hirooka Y 2017 *Fusion Eng. Des.* **125** 588
[16] Bi H and Hirooka Y 2017 *Fusion Eng. Des.* **125** 222
[17] Morley N B, Burris J, Cadwallader L C and Nornberg M D 2008 *Rev. Sci. Instrum.* **79** 056107
[18] Kiuchi K and McLellan R B 1983 *Acta Metallurgica* **31** 961
[19] McLellan R B 1983 *Scr. Metall.* **17** 1237
[20] Causey R A 2002 *J. Nucl. Mater.* **300** 91
[21] Onwudinanti C, Tranca I, Morgan T and Tao S 2019 *Nanomaterials (Basel)* **9** 129
[22] Woodruff D P and Horn K 1983 *Vacuum* **33** 633
[23] Rosseau L R S, Medrano J A, Bhardwaj R, Goetheer E L V, Filot I A W, Gallucci F and van Sint Annaland M 2022 *Membranes (Basel)* **12** 75
[24] Li S Y, Zhao W M, Qiao J H and Wang Y 2019 *Acta Phys. Sin.* **68** 217103 (in Chinese)
[25] Yen P S, Deveau N D and Datta R 2018 *Ind. Eng. Chem. Res.* **57** 1607
[26] Nazmutdinov R R and Zinkicheva T T 2004 *Russ. J. Electrochem.* **40** 379
[27] Mazayev S N and Prokofiev Y G 1994 *J. Nucl. Mater.* **212** 1497
[28] Zwolinski B J, Eyring H and Reese C E 1949 *J. Phys. Chem.* **53** 1426
[29] Marshakov A I, Rybkina A A and Skuratnik Y B 2000 *Russ. J. Electrochem.* **36** 1101
[30] Hoffman D, Singh B and Thomas III J H 1998 *Handbook of vacuum science and technology* (New York: Academic Press) pp. 1–812
[31] Kulsartov T V, Hayashi K, Nakamichi M, Afanasyev S E, Shestakov V P, Chikhray Y V, Kenzhin E A and Kolbaenkov A N 2006 *Fusion Eng. Des.* **81** 701
[32] Shestakov V Pisarev A Sobolev V Kulsartov S and Tazhibaeva I 2002 *J. Nucl. Mater.* **307** 1494
[33] Serra E, Perujo A and Benamati G 1997 *J. Nucl. Mater.* **245** 108
[34] Choi J Y 1970 *Metall Maaater. Trans. B* **1** 911
[35] Drexler A, Siegl W, Ecker W, Tkadletz M, Klösch G, Schnideritsch H, Mori G, Svoboda J and Fischer F D 2020 *Corros. Sci.* **176** 109017
[36] Swansiger W A, Wolfer W G and Baskes M I 1988 *J. Vac. Sci. Technol. A* **6** 1076
[37] Andrew P L and Haasz A A 1990 *J. Vac. Sci. Technol. A* **8** 1807
[38] Yamakawa K, Ege M, Hirscher M, Ludescher B and Kronmüller H 2005 *J. Alloys Compd.* **393** 5
[39] Hollmann E M and Pigarov A Y 2002 *Phys. Plasmas* **9** 4330
[40] Méndez I, Gordillo-Vázquez F J, Herrero V J and Tanarro I 2006 *J. Phys. Chem. A* **110** 6060
[41] Hirooka Y, Ohgaki H, Ohtsuka Y and Nishikawa M 2005 *J. Nucl. Mater.* **337–339** 585